Elemental biological imaging by differential absorption with a laser-produced x-ray source

Tillman, C; Mercer, I; Svanberg, Sune; Herrlin, K

Published in:
Journal of the Optical Society of America B: Optical Physics

DOI:
10.1364/JOSAB.13.000209

1996

Elemental biological imaging by differential absorption with a laser-produced x-ray source

C. Tillman, I. Mercer, and S. Svanberg

Division of Atomic Physics, Lund Institute of Technology, P.O. Box 118, S-221 00 Lund, Sweden

K. Herrlin

Department of Radiology, Lund University Hospital, S-221 85 Lund, Sweden

Received March 30, 1995; revised manuscript received June 12, 1995

We demonstrate the novel application of hard x rays emitted by a laser-produced plasma for differential imaging of elements. An x-ray-emitting laser-produced plasma, obtained by the focusing of radiation from a 10-Hz terawatt laser, is used for biological imaging. The x-ray source can be arranged to yield characteristic x-ray emission lines with photon energies that bridge the *K* absorption edge of a chosen atomic species. One can obtain element-specific radiographs by recording transillumination images for different target materials on digital image plates and by subsequently subtracting or dividing the images. Successful phantom and experimental animal imaging are performed utilizing tantalum and gadolinium as target materials for the terawatt laser and gadolinium as the imaged contrast agent. © 1996 Optical Society of America

1. INTRODUCTION

Spectroscopic imaging techniques can be applied to the production of two-dimensional images of specific elements or compounds. Specific images may be obtained directly for certain elements, e.g., radionuclides for scintigraphy or abundant nonzero nuclear-spin elements (notably hydrogen) in NMR imaging.[1]

An image may be enhanced by the subtraction of images, with one image being taken before and one after the administration of a contrast agent. This technique is applied in digital subtraction angiography[2,3] of human blood vessels and employs a standard x-ray tube as the radiation source. The injected contrast agent is flushed away within seconds, which puts a constraint on the maximum time that can elapse before recording of the second image. With monochromatic x-ray sources, however, it is possible in principle to perform image enhancement without constraints on the time delay between exposures. Two exposures are taken with x-ray photon energies above and below the absorption edge of the contrast agent. The essence of differential imaging is to subtract one image from the other, which results in an image in which the contrast agent is uniquely distinguished. Synchrotron radiation was used to perform such differential imaging[4–6]; however, this kind of x-ray source is costly, and the access is limited. In this paper we present differential x-ray absorption measurements based on a similar method, but we employ a compact radiation source for phantom and animal imaging. Two target materials were irradiated by a 10-Hz terawatt laser, producing characteristic line emission. There is the potential to combine differential imaging with two other attractive properties of a laser-produced plasma: (1) a very small source size (less than 60 μm in diameter) that permits high resolution and large projection magnification,[7,8] and (2) extremely short exposure times (thought to be of the order of picoseconds) that allow for time-gated viewing[9] and consequently a reduction in the radiation dose. The photon energy of the characteristic line emission from a laser-produced plasma can be changed by alteration of the target element. This capability permits the production of photon energies ranging from less than 1 keV to ~110 keV. An example of differential spectroscopic imaging, performed at optical wavelengths, is the mapping of atmospheric trace gases by differential absorption lidar,[10] in which the laser is tuned on and off an absorption line of the particular species.

In x-ray microscopy the so-called water window between the carbon and the oxygen *K* absorption edges (4.4 and 2.3 nm) provides a natural contrast between water (oxygen) and proteins (carbon).[11] However, radiation at this wavelength does not penetrate the depth of tissue that is of interest for medical imaging (>10 cm). Medical imaging requires the use of x rays of higher photon energy, combined with contrast agents with a higher atomic number, such as iodine or gadolinium, with the *K* absorption edges at the energies of 33 and 50 keV, respectively.

2. X-RAY ATTENUATION AND EMISSION

As a background for the present study on x-ray differential absorption imaging, we briefly summarize some basic aspects of absorption and emission. The attenuation of x rays in matter depends on both the x-ray photon energy and the atomic number of the absorbing material. The attenuation in an element smoothly decreases with photon energy until the photon energy is high enough to remove an electron from one of the electron shells. At this energy threshold the absorption increases abruptly because ionization from a new inner shell is permitted. The most prominent atomic absorption feature occurs for the innermost shell, giving rise to the *K* absorption edge.

0740-3224/96/010209-07$06.00

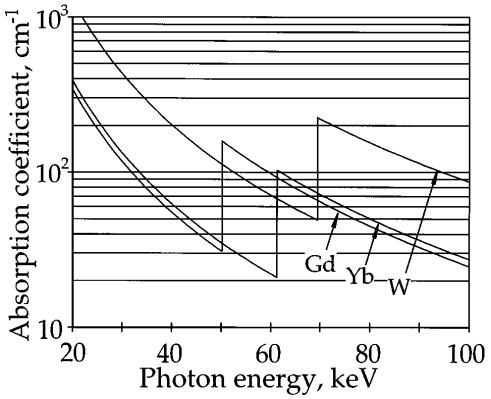

Fig. 1. Attenuation coefficient for three different elements in the 20–100-keV region. This diagram illustrates that an element can have an attenuation coefficient that is greater than that for a relatively heavier element in a certain region of the energy spectrum. The atomic numbers for the elements reported in the figure are $Z_{Gd} = 64$, $Z_{Yb} = 70$, and $Z_W = 74$. Tungsten has a relatively large absorption coefficient because of its higher density, being ~2.5 times the density of gadolinium and ytterbium.

Medical imaging requires the use of x rays that have a photon energy in the range of 20–120 keV, which deliver a sufficient image contrast while permitting high transmission through tissue. X-ray attenuation occurs by Compton scattering as well as by photoelectric conversion in this spectral region. Attenuation in this energy range increases with the cube of the atomic number, resulting in a significant difference in the absorption cross section for two elements even if they have closely related atomic numbers. However, with the inclusion of the effect of absorption edges, it is possible for an element to have a higher attenuation than a heavier element in a specific region of the energy spectrum (see Fig. 1).

The x-ray emission from a laser-produced plasma consists of both continuous bremsstrahlung and characteristic line emission.[12] The distribution of the bremsstrahlung spectrum is believed to be quite similar for different elements, whereas the photon energy of characteristic line emission is strongly dependent on the material in the plasma. It is straightforward to calculate the photon energy for different emission lines, as well as the position of the K absorption edge (Fig. 2), by means of the well-known Moseley law[12] with appropriate coefficients. It can be observed that the K absorption edge is situated closely above the K lines. Therefore the emission lines of an element have a low attenuation in the same element. In a plasma source in which many different ionization stages are present simultaneously, small fractional ionic shifts will make the actual spectral features complicated. However, these small shifts do not change the general discussion.

3. PRINCIPLES OF DIFFERENTIAL IMAGING

The general principle of differential imaging is to compare two or more digitally stored images that are exposed under different conditions. Comparison is usually made by division or subtraction of corresponding pixel values in the two images. Division is frequently favored because it yields a dimensionless quantity, and in this way variations in intensity and geometry are eliminated.

Differential imaging is very suitable for enhancement of small variations between two exposures and for suppressing information that remains the same for both images. In the case of radiological imaging, the differences introduced can result from motion, changed densities, added contrast media, or a changed spectral distribution of the source radiation. The method described in this paper is of the type in which the spectral energy distribution of x-ray radiation is changed between exposures.

Spectral characteristics can be manipulated without alteration of the source emission, e.g., by filtration; by use of scattered radiation; or by use of diffracting elements, such as crystals. One can directly manipulate the photon energy of the characteristic narrow-bandwidth radiation emitted by the source by changing the target material. The x-ray radiation used in the experiments described in this paper was filtered with aluminium, copper, and tantalum. For example, a 0.15-mm copper foil has an absorption of >90% at 25 keV, falling off fast at higher photon energies (<30% at 50 keV).

Biological samples consist mainly of light elements, e.g., hydrogen, oxygen, carbon, nitrogen, phosphor, and calcium, which have low absorption characteristics and K absorption edge energies less than 4.1 keV. Radiation with a photon energy of 4 keV can be estimated to have a $1/e$ transmission of approximately 0.2 mm in tissue. Therefore there is a need for heavier elements to be used as contrast agents, with the K absorption edges being at higher energies. Gadolinium was chosen as the contrast element for the following experiments because it has a K absorption edge at 50 keV. The use of x rays with photon energies in the region of 50 keV permits a high transmission in tissue ($1/e$ transmission depth, ~24 cm). Gadolinium is frequently used as a paramagnetic contrast agent in magnetic resonance imaging and is clinically approved.

One element used as the x-ray source should have its K emission lines below the energy of the K absorption edge of the contrast agent, and another element used should have its K emission lines above the K absorption edge. Gadolinium, which is used as the contrast agent, is also chosen as the target material, emitting characteristic radiation below its own K absorption edge. Tantalum was chosen as the second target material, with its K emission lines situated above the K absorption edge of

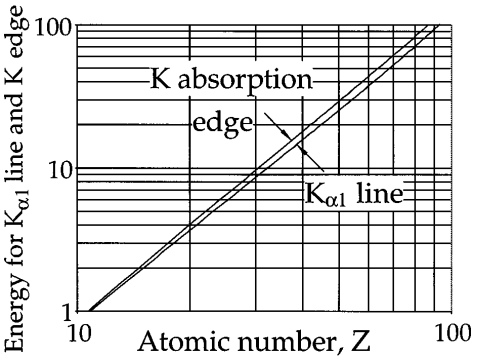

Fig. 2. Experimental data[13,14] for the photon energy of the $K_{\alpha 1}$ line and the K absorption edge versus the atomic number.

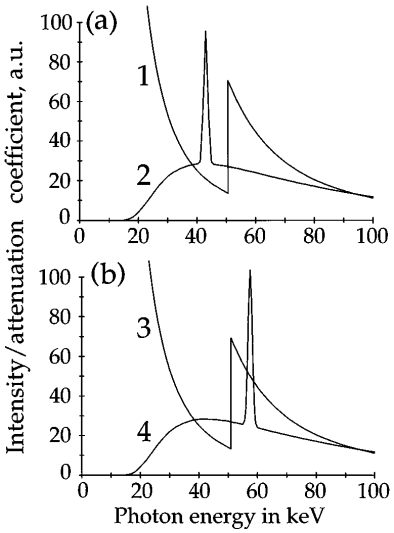

Fig. 3. Attenuation coefficient of gadolinium and simplified emission spectra. (a) 1. Attenuation coefficient in gadolinium, 2. emission from a gadolinium source filtered with 3 mm of aluminium. (b) 3. Attenuation coefficient in gadolinium, 4. emission from a tantalum source filtered with 3 mm of aluminium. The spectra are simplified, with only a single K line being plotted in each diagram.

gadolinium. In the general case, the characteristic radiation emitted by a gadolinium source is absorbed more than the characteristic radiation emitted by a tantalum source. However, when gadolinium itself is imaged, the transmission of the gadolinium characteristic lines is greater than the transmission of the tantalum characteristic lines (see Fig. 3). The method is made element selective by use of an absorption edge. The difference in absorption is larger if the K lines are moved nearer to the absorption edge. A few other elements could have offered photon energies closer to the K absorption edge in gadolinium, but these were not used because they are expensive.

Differential imaging, as described above, could be applied to microscopy. In such applications samples containing light elements could be interrogated with the use of characteristic x-ray emission with a lower photon energy.

4. EXPERIMENTAL SETUP

The laser used for the generation of x rays is a 10-Hz tabletop terawatt system based on chirped-pulse amplification in titanium-doped sapphire.[15] A mode-locked Ti:sapphire oscillator pumped by an argon-ion laser provides 100-fs pulses that are stretched in time by a factor of ~2500 with a diffraction grating stretcher.[16] The stretcher consists of two diffraction gratings and can be viewed as a frequency-dependent delay line. Stretching the pulse in time before amplification keeps the pulse power low enough to allow small-sized amplifiers to be used while avoiding optical damage. The pulses are injected into a Ti:sapphire regenerative amplifier by means of an intracavity Pockels cell. After amplification by a factor of 10^6 during 15 round trips of the regenerative amplifier cavity, the pulses are switched out by the Pockels cell. Final amplification is achieved in a four-pass Ti:sapphire amplifier pumped by ~1.3 J of radiation of 532 nm, supplied by two Nd:YAG lasers. After final amplification the diameter of the laser beam is increased to 50 mm so as not to damage optical components. The pulses are recompressed to 150 fs in another diffraction grating system, arranged so as to impart an equal and opposite frequency-dependent delay to that of the expander. The short pulse duration, together with a pulse energy of as much as 220 mJ, yields peak powers of more than 1 TW. An overview of the laser system is given in Fig. 4.

Ultrahigh intensities can cause a refractive-index change in air through interaction with the atomic nonlinear susceptibility.[16] This effect results in self-focusing, which may cause optical damage in mirrors and windows. Inside the experimental vacuum chamber, the 50-mm-diameter laser beam is focused by an $f/1$ off-axis parabolic mirror to an estimated diameter of a few micrometers. A separate measurement with a He–Ne laser permits focusing to a spot less than 2 μm in diameter. Gold-coated aluminium off-axis parabolic mirrors, with surface irregularities of less than $\lambda/5$ at 800 nm, are used for focusing the laser on the target, yielding intensities above 10^{18} W/cm^2. An equivalent refractive optic is not suitable because it would be ~1.5 cm thick, resulting in a large cumulative effect from the nonlinear refractive index of the material at the extremely high peak intensities. This effect results in self-phase modulation, which destroys the temporal and the spatial characteristics of the pulse.

A tantalum or gadolinium foil with a thickness of 0.25 mm is placed in the focus of the laser beam. Every laser pulse creates a dense plasma, burning a small crater in the target foil. The foil is glued to a steel disk that is slowly rotated and is translated in such a way that every new laser pulse interacts with a fresh area of the surface (see Fig. 5). Depending on the separation between the craters, one such disk will last for 1–2 h of operation at 10 Hz. If appropriate precautions are not taken, the ablated target material is deposited on the focusing optics. It was found that, by operation with a background pressure of approximately 20 mbar of air in the vacuum chamber, light particles are decelerated before reaching the surface of the focusing mirror. These particles do not stick to the surface, and one can easily remove them by blowing air across the mirror after opening the chamber. However, heavy particles more than 10 μm in diameter are permanently attached to an un-

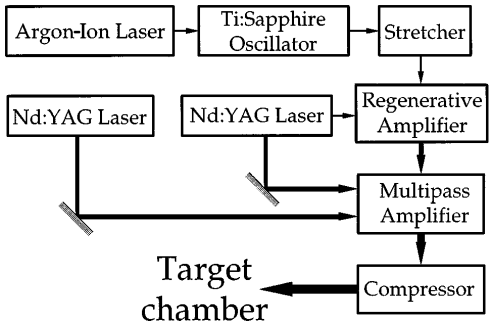

Fig. 4. A continuous-wave laser, pumping an oscillator, provides seed pulses that are amplified first in a regenerative amplifier and then by a large Ti:sapphire amplifier. The laser system delivers 150-fs pulses with a peak power of 1.5 TW at a rate of 10 Hz.

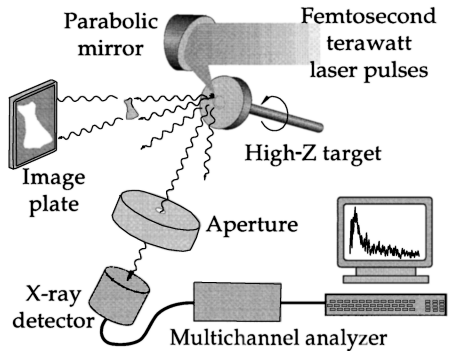

Fig. 5. Experimental setup. The 50-mm-diameter laser beam is focused by an $f/1$ off-axis parabolic mirror onto a rotating target. A standard glass microscope slide is inserted between the mirror and the target to protect the former from ablated material.

protected mirror surface, and after a few hours of operation the mirror has to be repolished and recoated. This problem was solved by the insertion of standard glass microscope slides (100 μm thick, 60 mm $\times$ 24 mm in size; Chance Propper Ltd., UK) between the mirror and the target surface. The efficiency of plasma and x-ray production is not significantly reduced by the insertion of the microscope slides.

Image plates were favored for the recording of x-ray images. These plates consist of a plastic substrate covered with an active 150-μm crystalline layer. Energy received as x rays is stored in the form of electron vacancies in the crystal lattice of the active material. Irradiation of the layer with laser light (He–Ne laser at 633 nm) leads to luminescence at a wavelength of ~400 nm.[17] The luminescence radiation is detected with a photomultiplier and is subsequently digitized.

Image plates have advantages over conventional x-ray films[17]:

- The sensitivity is greater by more than 1 order of magnitude.
- The dynamic range is 3 orders of magnitude greater (10^5).
- The response to x-ray dose is linear over the entire dynamic range.
- The accumulated background can be erased before use.
- The image plates can be reused after erasure of the previous exposure.
- Digitization and scanning of the plates is accomplished in just a few minutes.

The only disadvantages with the use of image plates is a limited resolution of 100 μm and a commercially unspecified spectral response. The measured luminescence signal is stored in logarithmic form, permitting effective storage of values extending over a dynamic range of several orders of magnitude. The stored image pixel values, Q, are given by the formula

$$Q = N\left[\frac{\log\left(\frac{IS}{\text{constant}}\right)}{L} + \frac{1}{2}\right], \tag{1}$$

where N is the number of gray-scale levels, I is the measured value of luminescence light, S is a sensitivity parameter, and L is a dynamic-range parameter.

Storage of values in a logarithmic format is convenient, as the subtraction of logarithms is equivalent to the operation of division on a linear scale. The operation of subtraction can be performed significantly faster than division, allowing image processing to be performed in seconds on a personal computer. It is also worth noting that the logarithm of exposure is proportional to the thickness, the concentration, and the absorption coefficient.

In the experiment we used imaging plates from Fuji (type BAS-III), together with a Fuji BAS-2000 system for scanning and digitization of the images. We used image plates measuring 20 cm$\times$ 40 cm in size for two exposures each, shadowing the unexposed area with lead bricks. Scanning with a resolution of 200 μm and a 10-bit gray scale yields image files of a size of ~4 MB.

A wide variety of solutions containing different elements were imaged so as to perform a controlled test of elemental imaging. Each of these solutions contains nitrate ions and water, with the major difference between solutions resulting from a change in a heavier element. The solutions were held in rectangular Plexiglas housings with cavities whose dimensions were 5 mm $\times$ 5 mm $\times$ 35 mm, sealed with 1-mm-thick Plexiglas windows attached to either side.

For a demonstration of a realistic application of this method to imaging in mammals, contrast media were inserted into two Wistar–Furth rats weighing ~200 grams and measuring ~150 mm in length. The preparation involved insertion of a plastic tube through the mouth and the esophagus down into the stomach and was performed by a medical expert. Aqueous solutions of 5 ml volume were placed in the stomach of each rat *post mortem*. One rat was administered a 2.27-M solution of $Gd[NO_3]_3 \cdot 6H_2O$; the other, a 2.27-M solution of $Ce[NO_3]_3 \cdot 6H_2O$.

5. GENERATION OF X RAYS FROM THE LASER-PRODUCED PLASMA

The optical axes of the focusing parabolic mirror has to be accurately aligned with respect to the laser beam so as to minimize the spatial extent of the focused laser spot on the rotating target. Removing the target and focusing the beam at air pressure creates a breakdown spark. With the laser producing only a few millijoules of laser light, the intensity of the spark is observed while the mirror is adjusted. One can align the mirror with an accuracy of ~2 mrad by gradually decreasing the laser energy while still trying to keep the spark as strong as possible. The rotating target is mounted into position again after alignment of the mirror. Movement of the target surface, i.e., wobbling, is caused by misalignment of the target surface relative to the rotational axis but is minimized by the turning of two adjustment screws. The vacuum chamber is evacuated to a pressure of ~20 mbar, a pressure low enough to avoid breakdown in air. A microscope slide is inserted between the mirror and the target so as to protect the target surface by blocking the fast particles sputtered away from the plasma. The laser power is increased to ~130 mJ, and the target is rotated

with a time of revolution of ~30 s, resulting in a typical separation of ~300 μm between the shots on the target. During operation, the target is moved sideways to expose new tracks for every revolution.

The rotating target can be moved in front of, or behind, the position of the laser focus. Blue light (the second harmonic of the fundamental laser wavelength of ~800 nm) is emitted when the target is moved more than ~200 μm in either direction from the position of best focus. The visible radiation emitted from the plasma changes to green (3/2 harmonic of the fundamental wavelength[18]) when the target is positioned appropriately, with the total x-ray yield from the plasma (measured with an ionization chamber) being roughly correlated to the flux of green light. However, the target position for the maximum yield of x rays is found to be ~100 μm closer to the focusing optic than the position required for maximum yield of green light.

The temporal duration of the emitted x rays is believed to be of the order of 1 ps,[19] and the energy distribution of the emitted x rays was measured with different detectors. Scintillating NaI detectors coupled to photomultiplier tubes show a limited resolution but reveal a photon energy tail extending above 1 MeV in accordance with previous results.[20] Germanium detectors in various configurations can offer a resolution corresponding to a value for $E/\Delta E$ of the order of 100. Energy-dispersive detectors are hampered by pileup, related to the finite recovery time of the detector, which leads to distorted spectra. Optional solutions for limiting the photon flux include passive filters, slits, and pinholes. A Compton spectrometer[12] was also used, consisting of a number of lead slits that block the primary x-ray beam but permit the passage of radiation scattered at 90° from a Lucite rod,[21] in combination with a germanium detector. Preliminary measurements showed a large content of characteristic line emission, compared with conventional x-ray tubes. Fluctuations in the production of x rays and the single-photon counting mode of these detectors place limits on the count rate during spectral recordings.

6. DIFFERENTIAL X-RAY IMAGING

Exposures were made with the use of gadolinium and tantalum as x-ray radiation sources. A 0.1-mm-thick tantalum foil was used as a filter, effectively removing soft x rays with a residual transmission of 3×10^{-5} at 20 keV and of 38% at 50 keV. Test phantoms and metal foils were placed directly in front of an image plate. An exposure was made of the test objects with a tantalum plasma x-ray source [see Fig. 6(a)], and a similar image was recorded with a gadolinium plasma x-ray source. When viewed separately, the two images appear to be similar. Customized computer software was developed for dividing the two images. The pixel values from the gadolinium-source exposure were divided by the pixel values from the tantalum-source exposure, with the result being stored in logarithmic form, showing exposure values that are dependent on element concentrations [see Fig. 6(b)]. Solutions containing gadolinium are lighter in the divided image, corresponding to a ratio between the exposures that is greater than the ratio of unfiltered regions. Solutions containing other elements with high absorption are darker in the image, corresponding to a ratio between the exposure values that is less than the ratio of unfiltered regions. The differential effect increases with the concentration of the solutions. A similar result can be observed for metal foils [see Figs. 7(a) and 7(b)]. In the differential image shown in Fig. 6(b), the transmission ratios for solutions 22 (cerium), 7 (gadolinium), 3 (ytterbium), and 19 (tungsten) are 0.97, 1.03, 0.98, and 0.97, respectively. A theoretical calculation of the

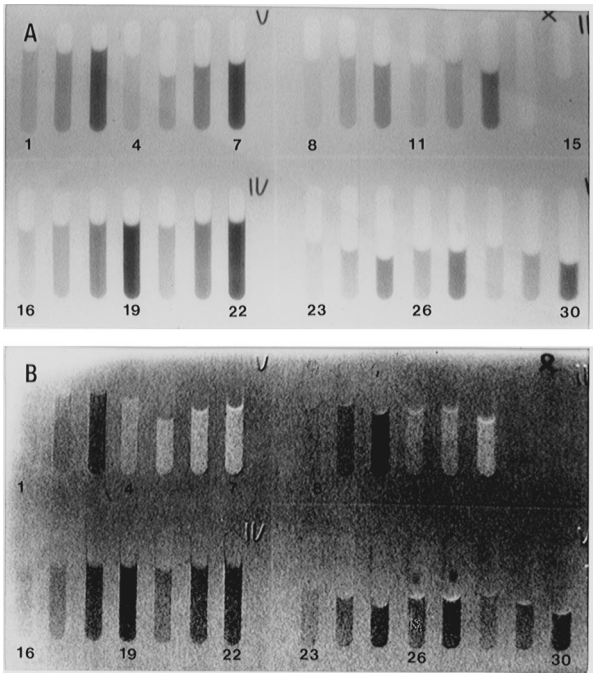

Fig. 6. (a) X-ray image of test phantoms containing solutions. The exposure was made with a gadolinium radiation target. From the left, the labeled tubes are as follows. Top rows: 1–3, ytterbium; 4–7, gadolinium; 8–10, cerium; 11–13, gadolinium; 14, air; 15, pure water. Bottom row: 16–19, tungsten; 20–22, cerium; 23–25, caesium; 26–27, barium; 28–30, lead. When more than one sample of each element was used, the concentration in the samples increases from the left to the right in the image. (b) Differential image of the same object as in (a). The pixel values from an exposure with a gadolinium source was divided by the pixel values for an exposure by use of a tantalum source, with the result being stored in logarithmic form.

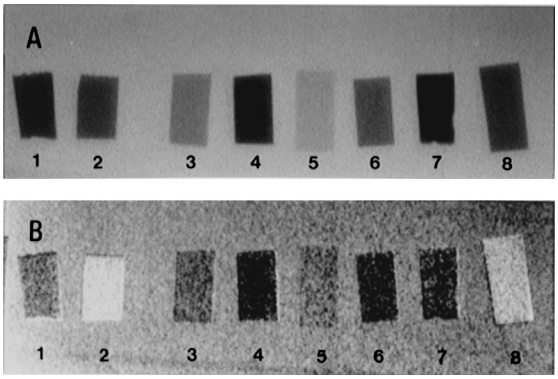

Fig. 7. (a) X-ray image of metal foils. The exposure was made with a gadolinium radiation target. From the left, the labeled foils are as follows. 1, tin; 2, gadolinium; 3, molybdenum; 4, tantalum; 5, nickel; 6, unknown; 7, tin; and 8, gadolinium. (b) Differential image of the same foils as in (a), with the gadolinium radiation source used in (a) and a tantalum radiation source.

transmission ratios for these solutions was performed with tabulated values for x-ray attenuation[13] and assuming monochromatic radiation from the $K_{\alpha 1}$ lines (the strongest lines) in gadolinium and tantalum. It was assumed that the solutions contained pure elements, and the attenuation of Plexiglas, water, and nitrate ions was neglected. The theoretical transmission ratios for solutions 22 (cerium), 7 (gadolium), 3 (ytterbium), and 19 (tungsten) were 0.11, 4.3, 0.56, and 0.24, respectively. There is a large difference in magnitude between the experimental and the simulated transmission values; however, there is a significant correlation between the two. These results indicate that, in the experiment, certain phenomena are effective in reducing the contrast of the differential image, the most significant of which is believed to be broadband x-ray emission from the source. Theoretical values are calculated assuming monochromatic x-ray radiation, but the experimental values are measured with an x-ray source emitting both characteristic line emission and a bremsstrahlung continuum. Photons with energies outside the energy range defined by the K absorption edge in gadolinium and by the K absorption edge in tantalum will bring the value of the transmission ratios closer to that for the ratio of unfiltered regions. Monochromatic x-ray radiation and a low scattering background result in higher contrast, allowing the concentration of the contrast agent to be lowered to medically acceptable values. Simulations show that, with the use of monochromatic x-ray radiation, the contrast obtained in our recording can be achieved with approximately 1/50 of the elemental concentration.

The four elements in the calculations discussed above were selected because of the value of the energies of their K absorption edges relative to the K emission lines in the radiation source elements. Three different cases have to be investigated: (1) The energy of the K absorption edge has a value below all the K emission lines in the two target elements. (2) The energy of the K absorption edge has a value between the K emission lines of the first target element and the K emission lines of the second target element. (3) The energy of the K absorption edge has a value above all the K emission lines in the two target elements. With gadolinium and tantalum as target elements, cerium applies to case 1, gadolinium applies to case 2, and tungsten applies to case 3. Ytterbium does not fit in any of these three cases because its energy of the K absorption edge has a value higher than the K emission lines of gadolinium and the K_{α} emission lines of tantalum but lower than the K_{β} emission lines of tantalum, which is reflected by its higher transmission ratio compared with cerium and tungsten.

7. ANIMAL IMAGING

An application of differential imaging *in vivo* was performed with the use of experimental animals. Two images were recorded with x rays produced by means of the same target setup as described in Section 6 [see Fig. 8(a)]. The radiation was filtered with a 0.45-mm copper foil. The image processing was done in the same manner as with the solutions. The resulting differential image [see Fig. 8(b)] shows that the stomach of the mammal shown on the left (which contains cerium) appears darker than the surrounding tissue and that the stomach of the mammal shown on the right (which contains gadolinium) appear lighter than the surrounding tissue. This result is in agreement with the results of the research performed with solutions and filters.

8. DISCUSSION

Synchrotron-assisted digital subtraction angiography allows for a reduction in the x-ray dose for the examined patients.[4,22] A dose reduction can also be realized by use of a laser-produced plasma. Time-gated viewing in combination with differential imaging could reduce the radiation dose needed to deliver the required image contrast by suppression of background radiation. In a previous study it was estimated that time-gated viewing could allow for a dose reduction of as much as a factor of 8.[9] The principle of time-gated viewing is the same as that applied to transillumination utilizing visible or infrared radiation.[23] Ballistic photons have a shorter path length in tissue compared with scattered photons, and, with the use of a time-gated detector, scattered photons may be blocked.

It is desirable to use narrow-bandwidth radiation when performing medical imaging, so that image contrast can be maximized while the radiation dose is minimized, resulting in a corresponding improvement in radiation safety. It is also desirable to remove low-photon-energy radiation because it is mostly absorbed and therefore can be responsible for a major portion of the absorbed patient dose.[24] Metal filters are used for the suppression of low photon energies, e.g., a few millimeters of aluminium. The major form of attenuation of high-photon-energy radiation is through Compton scattering rather than through absorption by photoelectric conversion. Scattering of the x-ray radiation does not contribute to useful

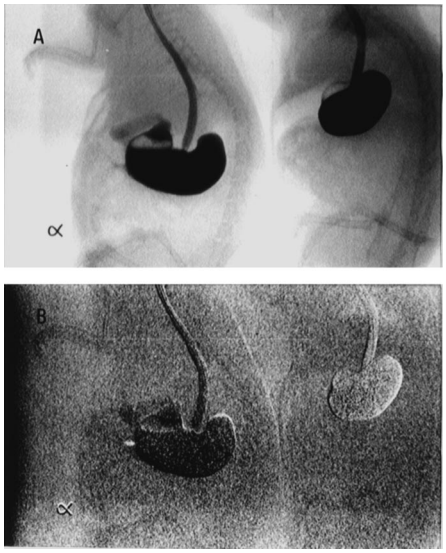

Fig. 8. (a) X-ray image showing two rats viewed from the left-hand side. The stomach of each rat was prepared with a solution of cerium (left) and gadolinium (right). The exposure was made by means of a tantalum radiation target. (b) Differential image with the same view as in (a). Two exposures were made, one with the tantalum radiation source used in (a) and one with a gadolinium radiation source. Each exposure was made for a period of 1 min.

information; instead, it increases the noise level at the detector. However, it may be possible to remove the effects of scattered radiation with the application of time-gated viewing.

It has been shown that the small monochromatic x-ray source described in this paper can be applied to differential imaging. Although differential images achieved with x rays from synchrotron sources are superior in image quality, x-ray sources other than exclusive synchrotrons are required for the technique to become widespread. The new x-ray source may also allow for the application of time-gated viewing, leading to a reduction in the x-ray dose and thereby to an improvement in radiation safety. Rapid development in laser technology will lead to smaller and more powerful lasers, which will permit production of even brighter plasma sources. The concentration of the contrast agent can be strongly reduced by use of spectrally brighter x-ray sources, permitting realistic medical imaging.

ACKNOWLEDGMENTS

This project has been supported by the Swedish Medical Research Council and by the Crafoord Foundation and has been conducted as part of a program of studies of hard x rays from laser-produced plasmas. The program has been funded by the Swedish Natural Sciences Research Council and the Human Capital and Mobility Programme (contract CHRX-CT93-0346). The authors thank C. Andersson, B. Erlandsson, M. Grätz, C.-G. Wahlström, A. Persson, H. Petterson, G. Svahn, and C. Olsson for valuable discussions and assistance. Animals for the experiment were prepared by D. L. Liu. Nycomed Innovation AB has been helpful in supplying contrast enhancement substances.

REFERENCES

1. R. S. MacKay, *Medical Images and Displays: Comparisons of Nuclear Magnetic Resonance, Ultrasound, X-Rays and Other Modalites* (Wiley, New York, 1984).
2. P. Maher and J. F. Malone, "Digital fluoroscopy: a new development in medical imaging," Contemp. Phys. **27,** 533–552 (1986).
3. W. R. Brody, *Digital Radiography* (Raven, New York, 1984), Chap. 10, pp. 105–158.
4. W. Thomlinson, N. Gmür, D. Chapman, R. Garret, N. Lazarz, H. Moulin, A. C. Thompson, H. D. Zeman, G. S. Brown, J. Morrison, P. Reiser, V. Padmanabahn, L. Ong, S. Green, J. Giacomini, H. Gordon, and E. Rubenstein, "First operation of the medical research facility at the NSLS for coronary angiography," Rev. Sci. Instrum. **63,** 625–628 (1992).
5. N. F. Gmür, D. Chapman, W. Thomlinson, A. C. Thompson, W. M. Lavender, K. Scalia, N. Malloy, J. Mangano, and J. Jacob, "NSLS transvenous coronary angiography beamline upgrade and advanced technology initiatives," Rev. Sci. Instrum. **66,** 1357–1360 (1995).
6. A. C. Thompson, W. M. Lavender, D. Chapman, N. Gmür, W. Thomlinson, V. Rosso, C. Schulze, E. Rubenstein, J. C. Giacomini, H. J. Gordon, and J. P. Dervan, "A 1200 element detector system for synchrotron-based coronary angiography," Nucl. Instrum. Methods Phys. Rev. A **347,** 545–552 (1994).
7. K. Herrlin, G. Svahn, C. Olsson, H. Pettersson, C. Tillman, A. Persson, C.-G. Wahlström, and S. Svanberg, "Generation of x-rays for medical imaging by high-power lasers: preliminary results," Radiology **189,** 65–68 (1993).
8. C. Tillman, A. Persson, C.-G. Wahlström, S. Svanberg, and K. Herrlin, "Imaging using hard x-rays from a laser-produced plasma," Appl. Phys. B **61,** 333–338 (1995).
9. C. L. Gordon III, G. Y. Yin, B. E. Lemoff, P. M. Bell, and C. P. J. Barty, "Time-gated imaging with an ultrashort-pulse, laser-produced-plasma x-ray source," Opt. Lett. **20,** 1056–1058 (1995).
10. S. Svanberg, "Differential absorption lidar (DIAL)," in *Air Monitoring by Spectroscopic Techniques*, M. Sigrist, ed. (Wiley, New York, 1994), Chap. 6, pp. 85–161.
11. A. G. Michette, G. R. Morrison, and C. J. Buckley, eds., *X-ray Microscopy III*, Vol. 67 of Springer Series in Optical Sciences (Springer, Berlin, 1992).
12. B. Cagnac and J. C. Pebay-Peyroula, *Modern Atomic Physics—Fundamental Principles* (Macmillan, London, 1975), Chap. 7, pp. 168–190.
13. W. M. J. Veigele, "Photon cross sections from 0.1 keV to 1 MeV for elements $Z = 1$ to $Z = 94$," At. Data Tables **5,** 51–100 (1973).
14. C. M. Lederer and V. S. Shirley, eds., *Table of Isotopes*, 7th ed. (Wiley, New York, 1978), Apps. 11 and 12.
15. S. Svanberg, J. Larsson, A. Persson, and C.-G. Wahlström, "Lund High-Power Laser Facility–systems and first results," Phys. Scr. **49,** 187–197 (1994).
16. A. E. Siegman, *Lasers* (University Science, Mill Valley, Calif., 1986), Chap. 9, pp. 349, 380–381.
17. J. Miyahara, "The imaging plate: a new radiation image sensor," Chem. Today **223,** 29–36 (October 1989).
18. D. Giulietti, V. Biancalanca, D. Batani, A. Giulietti, L. Gizzi, L. Nocera, and E. Schifano, "Three-half harmonic generation in laser–plasma interaction: evidence for plasmon generation," Nuovo Cimento **13,** 845–858 (1991).
19. J. C. Kieffer, M. Chaker, C. Y. Côte, Y. Beaudoin, H. Pépin, C. Y. Chien, S. Coe, and G. Mourou, "Time-resolved kiloelectron-volt spectroscopy of ultrashort plasmas," Appl. Opt. **32,** 4247–4252 (1993).
20. J. D. Kmetec, C. L. Gordon III, J. J. Macklin, B. E. Lemoff, G. S. Brown, and S. E. Harris, "MeV x-ray generation with a femtosecond laser," Phys. Rev. Lett. **68,** 1527–1530 (1992).
21. G. Matscheko, "A Compton scattering spectrometer," Ph.D. dissertation (Linköping Univ., Linköping, Sweden, 1988).
22. J. M. Boone and J. A. Seibert, "A figure of merit comparison between bremsstrahlung and monoenergetic x-ray sources for angiography," J. X-ray Sci. Technol. **4,** 334–345 (1994).
23. G. Müller, B. Chance, R. Alfano, S. Arridge, J. Beuthan, E. Gratton, M. Kaschke, B. Masters, S. Svanberg, and P. van der Zee, eds., *Medical Optical Tomography: Functional Imaging and Monitoring* (Society of Photo-Optical Instrumentation Engineers, Bellingham, Washington, 1993), Vol. IS11.
24. F. Carroll, "Use of monochromatic x-rays in medical diagnosis and therapy—What is it going to take?" J. X-ray Sci. Technol. **4,** 323–333 (1994).